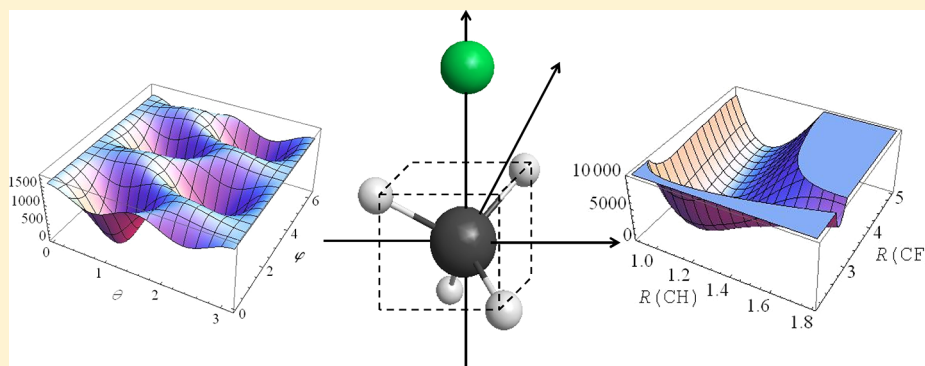


Reduced-Dimensional Quantum Computations for the Rotational–Vibrational Dynamics of F^-CH_4 and $F^-CH_2D_2$

Csaba Fábri, Attila G. Császár, and Gábor Czakó*

Laboratory of Molecular Structure and Dynamics, Institute of Chemistry, Eötvös University, H-1518 Budapest 112, P.O. Box 32, Hungary



ABSTRACT: Variational rotational–vibrational quantum chemical computations are performed for the F^-CH_4 and $F^-CH_2D_2$ anion complexes using several reduced-dimensional models in a curvilinear polyspherical coordinate system and utilizing an accurate ab initio potential energy surface (PES). The implementation of the models is made practical by using the general rovibrational code GENIUSH, which constructs the complicated form of the exact rovibrational kinetic energy operator in reduced and full dimensions in any user-specified coordinates and body-fixed frames. A one-dimensional CF stretch, $1D(R_{CF})$, a two-dimensional intermolecular bend, $2D(\theta, \varphi)$, and a three-dimensional intermolecular, $3D(R_{CF}, \theta, \varphi)$, rigid methane model provide vibrational energies for the low-frequency, large-amplitude modes in good agreement with full-dimensional MCTDH results for F^-CH_4 . The $2D(\theta, \varphi)$ and $3D(R_{CF}, \theta, \varphi)$ four-well computations, describing equally the four possible CH– F^- bonds, show that the ground-state tunneling splitting is less than 0.01 cm^{-1} . For the hydrogen-bonded CH stretching fundamental a local-mode model is found to have almost spectroscopic accuracy, whereas a harmonic frequency analysis performs poorly. The $2D(\theta, \varphi)$ and $3D(R_{CF}, \theta, \varphi)$ rotational–vibrational computations on the T_d -symmetric four-well PES reveal that in most cases F^-CH_4 behaves as a semirigid C_{3v} , symmetric top. For the degenerate intermolecular bending vibrational states substantial splittings of the rigid rotor levels are observed. For $F^-CH_2D_2$ the rotational levels guide the assignment of the vibrational states to either F^-H or F^-D connectivity.

■ INTRODUCTION

Molecular complexes stabilized by secondary interactions play an important role in chemistry. The simplest complexes are composed of two monomers. Pre- and postreactive dimer complexes are often formed in bimolecular chemical reactions, and these complexes sometimes have significant effects on the reaction dynamics.^{1–3} Recently, several experimental and theoretical studies focused on the $F + \text{methane}$ (CH_4 , CHD_3 , etc.) reaction providing new and sometimes unexpected insights into fundamental rules governing chemical reactivity.^{4–8} Recent dynamical computations suggest that the prereactive van der Waals forces between the reactants, methane and the F atom, are responsible for the surprising outcome, i.e., enhancement of the $DF + CHD_2$ channel by exciting the CH stretch of CHD_3 , of this fundamental polyatomic reaction.¹ The neutral F –methane complex is very unstable; its dissociation energy (D_e) is only around 160 cm^{-1} .⁹ Methane binds the F^- anion much more strongly; the computed D_e and D_0 values of F^-CH_4 are 2398 ± 12 and

$2280 \pm 20 \text{ cm}^{-1}$, respectively.¹⁰ Thus, the F^-CH_4 anion complex can be investigated spectroscopically more straightforwardly. Early experimental work probed F^-CH_4 in the CH stretching region, reporting a CH stretching fundamental of 2535 cm^{-1} , red-shifted by 382 cm^{-1} relative to the $\nu_1(a_1)$ mode of the CH_4 monomer.^{11–13} Note that a harmonic frequency analysis seriously overestimates this hydrogen-bonded CH fundamental, by about 250 cm^{-1} . The stable anion complex offers an efficient way to probe the neutral system via photodetachment spectroscopy.¹⁴ Recently, the F^-CH_4 anion has been used as a precursor to probe the entrance channel of the $F + CH_4$ reaction.^{15,16} The anion has a single hydrogen-bonded C_{3v} equilibrium structure, which slightly

Special Issue: Joel M. Bowman Festschrift

Received: December 10, 2012

Revised: February 9, 2013

Published: February 12, 2013

overlaps with the geometry of the transition state of the neutral reactive system;¹⁵ thus, this important region of the reactive potential energy surface (PES) can be directly investigated experimentally.

The first full-dimensional *ab initio* PES of the F^-CH_4 complex was reported by Czakó, Braams, and Bowman¹⁰ (CBB) in 2008, on the basis of a permutationally invariant fit to a large number of CCSD(T)/aug-cc-pVTZ energy points. Vibrational configuration interaction calculations performed using the code Multimode¹⁷ and the CBB PES¹⁰ gave 2519 cm^{-1} ¹⁰ for the above-mentioned red-shifted CH fundamental, in good agreement with experiment (2535 cm^{-1}).¹¹ Multimode employs the Eckart–Watson^{18,19} Hamiltonian and rectilinear normal coordinates; therefore, it cannot describe the tunneling dynamics between the four equivalent minima of the PES. Furthermore, the use of rectilinear coordinates may result in slow convergence for the low-frequency intermolecular modes. In 2012, multiconfigurational time-dependent Hartree (MCTDH)^{20,21} computations utilizing curvilinear stereographic coordinates were performed in full dimensions to investigate the multiwell dynamics of F^-CH_4 on the CBB PES.²² The MCTDH study provided benchmark vibrational energy levels for the intermolecular modes and the seemingly unconverged computations resulted in tunneling splittings on the order of 1 cm^{-1} .²² Because the MCTDH approach converges the vibrational energies from bottom to top, the full-dimensional computation of intramolecular vibrations is currently not feasible.²²

In the present work we investigate the multiwell rotational–vibrational dynamics of F^-CH_4 and $F^-CH_2D_2$, employing several reduced-dimensional quantum chemical models. The computations are performed using the fourth-age²³ code GENIUSH, a general (GE) rovibrational code with numerical (N), internal-coordinate (I), user-specified Hamiltonians (USH).^{24,25} Rigid monomer models are frequently used to study the large-amplitude intermolecular vibrations of van der Waals complexes.^{26–28} For F^-CH_4 we can test the performance of various reduced-dimensional models by comparing the GENIUSH results with the full-dimensional MCTDH reference data. Furthermore, we perform for the first time computations with nonzero total angular momentum, characterized by the quantum number J corresponding to the overall rotation of the system. It is an interesting question whether F^-CH_4 behaves as a symmetric top rotor, as expected from the C_{3v} equilibrium structure(s), or the rotational states correspond to a spherical top, reflecting the $T_d(M)$ molecular symmetry of the four-well PES. Finally, we present the first rovibrational results for the $F^-CH_2D_2$ complex allowing the investigation of isotope effects and, even more importantly, the consequences of changing the point-group symmetry of the methane fragment.

METHODS

A general form of the rotational–vibrational Hamiltonian of a molecule with D vibrational degrees of freedom can be written as^{29,30,24,25}

$$\hat{H} = \frac{1}{2} \sum_{k=1}^{D+3} \sum_{l=1}^{D+3} \tilde{g}^{-1/4} \hat{p}_k^+ G_{kl} \tilde{g}^{-1/2} \hat{p}_l \tilde{g}^{-1/4} + \hat{V} \quad (1)$$

where $\tilde{g} = \det(\mathbf{g})$, \mathbf{g} is the mass and coordinate dependent rotational–vibrational metric tensor, $\mathbf{G} = \mathbf{g}^{-1}$, \hat{p}_k 's are the quasi-momenta, and \hat{V} is the potential energy operator. GENIUSH numerically constructs the exact kinetic energy operator in any

user-specified coordinate system and body-fixed frame and computes the rovibrational states using a discrete variable representation (DVR)³¹ and an iterative Lanczos³² eigensolver. The reduced-dimensional models are defined by fixing coordinates and deleting the corresponding rows and columns of the \mathbf{g} matrix. It is important to note that the constraints should be introduced in the \mathbf{g} matrix before its inversion, because this corresponds to physically fixing coordinates, whereas reducing the \mathbf{G} matrix means constraining the momenta. The converged results obtained by the former approach, used in the present study, do not depend on the choice of the active coordinates, whereas the latter constraint can result in different energy levels depending on the coordinate system employed.²⁴

For the F^-CH_4 and $F^-CH_2D_2$ complexes we use curvilinear polyspherical coordinates, which are well suited to describe the motion of F^- around the methane unit. For the radial coordinates we employ potential-optimized DVR^{33–35} (PO–DVR) based on a primitive Laguerre–DVR. For the angles $\theta \in [0, \pi]$ and $\varphi \in [0, 2\pi]$ Legendre- and Fourier–DVR are employed, respectively. Because the two-dimensional angular motion of F^- is fully coupled, we found that PO–DVRs based on one-dimensional effective potentials are not efficient for θ and φ ; therefore, we used primitive grids for the angles. For the $J > 0$ rovibrational computations a rotational basis of $2J + 1$ orthonormal Wang functions²⁵ is employed. Convergence of the energy levels was carefully tested and we found that 20 radial PO–DVR points and 80 points for each angular coordinate are usually sufficient to converge the energies investigated in the present study to better than 0.01 cm^{-1} .

We are considering the following reduced-dimensional models (note that the dimensions of the models refer to the active vibrational coordinates only; thus, for $J > 0$ computations three additional rotational dimensions exist):

One-Dimensional Intermolecular Stretching, 1D(R_{CF}), Model. As shown in Figure 1, all the constrained coordinates

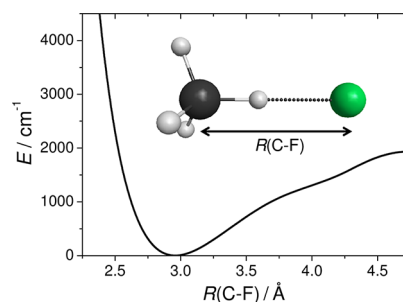


Figure 1. One-dimensional intermolecular stretching model of F^-CH_4 .

are kept frozen at their equilibrium values and the F^- ion can move in one dimension along the C_3 axis. For $F^-CH_2D_2$ two different 1D(R_{CF}) models are defined, in which either an H or a D atom is connected to F^- .

Two-Dimensional Intermolecular Bending, 2D(θ, φ), Model. The 2D(θ, φ) model is obtained by fixing the CF distance at its equilibrium value of 2.958 Å and treating CH_4 as a rigid monomer with T_d symmetry and a CH bond length of 1.104 Å. The T_d symmetry of the CH_4 unit was kept to exactly maintain the equivalence of the four minima in a rigid monomer model. This is a reasonable approximation, because

at the C_{3v} equilibrium structure of F^-CH_4 the two different types of CH distances differ by only 0.017 Å and the bond angle is distorted by only 1° from the exact tetrahedral angle.¹⁰ For the $F^-CH_2D_2$ complex the geometry of the rigid methane subunit was unchanged, we just replaced two H atoms with D atoms. Note that, in principle, in the $2D(\theta, \varphi)$ model all the hydrogen atoms are equivalent. However, we found that it is practical to define a body-fixed frame in which the hydrogen atoms are at the vertices of a cube and the three orthogonal axes are perpendicular to the faces of the cube (Figure 2). This

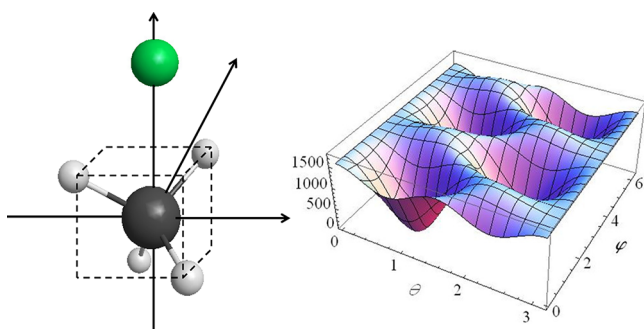


Figure 2. Two-dimensional $2D(\theta, \varphi)$ and three-dimensional $3D(R_{CF}, \theta, \varphi)$ models of F^-CH_4 . In the body-fixed frame the F^- is at $\theta = 0$ and $\varphi = 0$. (Note that in the actual computations the system is moved into the center of mass frame.) The $2D(\theta, \varphi)$ potential (energies in cm^{-1} and angles in radians) was obtained by fixing R_{CF} at 2.958 Å and treating CH_4 as a rigid monomer with T_d symmetry and a CH distance of 1.104 Å.

way the Legendre- and Fourier-DVR points, which are symmetric to 90° and 180° , respectively, describe the motion of F^- over the four equivalent minima (Figure 2) with the same precision. This was tested for $F^-CH_2D_2$, where we found that any permutation of the HHDD atoms resulted in the same energy levels.

Three-Dimensional Intermolecular, $3D(R_{CF}, \theta, \varphi)$, Model. In the $3D(R_{CF}, \theta, \varphi)$ model all the intermolecular coordinates are active; thus, this model corresponds to the rigid monomer models frequently used to study van der Waals dimers. The properties of this model are similar to those of the above-described $2D(\theta, \varphi)$ model seen in Figure 2, except that in the $3D(R_{CF}, \theta, \varphi)$ model the R_{CF} coordinate is also active.

One-Dimensional CH Stretching, $1D(R_{CH})$, Model. As shown in Figure 3, in this intramolecular stretching model all the constrained coordinates are kept frozen at their equilibrium values and the H-bonded H atom can move in one dimension along the C_3 axis. For $F^-CH_2D_2$ two different models,

$1D(R_{CH})$ and $1D(R_{CD})$, are defined, in which either the active H or D atom is connected to F^- , respectively.

Two-Dimensional CH–F Stretching, $2D(R_{CH}, R_{CF})$, Model. In the $2D(R_{CH}, R_{CF})$ model the H-bonded CH and CF stretchings are active along the C_3 axis and all the other coordinates are constrained at their equilibrium values. The resulting $2D(R_{CH}, R_{CF})$ PES is shown in Figure 3. Note that the radial PO–DVR points were set to satisfy the $R_{CH} < R_{CF}$ condition. Similar to the former model, for $F^-CH_2D_2$ two different models, $2D(R_{CH}, R_{CF})$ and $2D(R_{CD}, R_{CF})$, are defined, in which F^- is connected to either the active CH or CD bond, respectively.

RESULTS AND DISCUSSION

After the above-described reduced-dimensional models have been implemented into GENIUSH,^{24,25} variational rovibrational computations have been performed for the F^-CH_4 and $F^-CH_2D_2$ complexes using the CBB PES.¹⁰

Intermolecular Vibrations. The intermolecular vibrational energy levels for several models are presented in Table 1. For F^-CH_4 the $1D(R_{CF})$ model gives an intermolecular stretching fundamental (ν_s) of 193.6 cm^{-1} , in excellent agreement with the 12D benchmark result²² of 194.4 cm^{-1} . Anharmonicity has a small effect on ν_s , because the harmonic value is 200 cm^{-1} .¹⁰ In the $1D(R_{CF})$ model the transitions $\nu_s \rightarrow 2\nu_s$ and $2\nu_s \rightarrow 3\nu_s$ are 184.8 and 175.4 cm^{-1} , respectively; thus, again only a slight anharmonicity is seen. The $3D(R_{CF}, \theta, \varphi)$ model gives a ν_s of 182.5 cm^{-1} , slightly underestimating the 12D result. For the intermolecular bending fundamental (ν_b) the $2D(\theta, \varphi)$ and $3D(R_{CF}, \theta, \varphi)$ models yield 290.2 and 284.5 cm^{-1} , respectively, whereas the 12D benchmark result is around 272 cm^{-1} . Due to some error cancellation, the $3D(R_{CF}, \theta, \varphi)$ $\nu_s + \nu_b$ combination band at 459 cm^{-1} is in good agreement with the 12D result of 461 cm^{-1} .

For the intermolecular modes we can expect slow convergence when we employ Multimode, a code based on the Eckart–Watson operator and thus on rectilinear normal coordinates. Indeed, Multimode provides ν_b energies of 347, 314, 306, and 300 cm^{-1} using 1820, 6188, 17640, and 21348 basis functions, respectively.¹⁰ Knowing the 12D MCTDH result²² of 272 cm^{-1} and the present $3D(R_{CF}, \theta, \varphi)$ result of 285 cm^{-1} , we can conclude that even the largest basis set used in ref 10 was not sufficient to provide a converged result for the ν_b mode (of course, the above convergence test taken from ref 10 suggested this). Note that Multimode uses an approximate n -mode representation (n MR) of the PES and the inverse of the effective moment of inertia, but this n MR converges rapidly with increasing n and as ref 10 shows the 4MR and 5MR ν_b

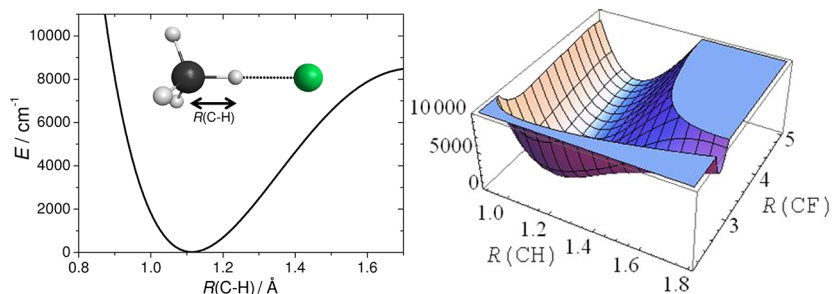


Figure 3. One-dimensional CH stretching, $1D(R_{CH})$, and two-dimensional CH–F stretching, $2D(R_{CH}, R_{CF})$, models of F^-CH_4 . The $1D(R_{CH})$ and $2D(R_{CH}, R_{CF})$ potentials (energies in cm^{-1} and distances in Å) were obtained by fixing all the nonactive coordinates at their equilibrium values.

Table 1. Intermolecular Vibrational Energy Levels (cm^{-1}) of the $\text{F}^- - \text{CH}_4$ and $\text{F}^- - \text{CH}_2\text{D}_2$ Complexes^a

	$\text{F}^- - \text{CH}_4$				$\text{F}^- - \text{CH}_2\text{D}_2$		
	1D(R_{CF})	2D(θ, φ)	3D($R_{\text{CF}}, \theta, \varphi$)	12D ^b	1D(R_{CF})	2D(θ, φ)	3D($R_{\text{CF}}, \theta, \varphi$)
ν_0	0.00	0.00	0.00	0.0	0.00	0.00	0.00
		0.00	0.00	0.6		0.00	0.00
		0.00	0.00	0.8		19.12	19.11
		0.00	0.00	0.9		19.12	19.11
ν_s	193.55		182.46	194.4	187.90		177.87
			182.46	194.4			177.87
			182.46	194.5			196.75
			182.46	194.5			196.75
ν_b		290.20	284.54	271.7		226.30	223.70
		290.20	284.55	271.7		226.30	223.70
		290.20	284.55	271.7		248.92	244.49
		290.20	284.55	271.8		248.92	244.49
		290.20	284.55	271.9		259.38	254.82
		290.20	284.55	272.4		259.39	254.82
		290.21	284.55	272.5		287.22	283.76
		290.21	284.56	272.8		287.22	283.76
$2\nu_s$	378.36		355.82	380.6	367.60		347.49
			355.82	380.7			347.49
			355.82	380.7			366.05
			355.82	380.7			366.05
$\nu_s + \nu_b$			458.81	460.2			395.22
			458.81	460.3			395.22
			458.81	460.4			415.63
			458.81	460.4			415.63
			458.81	461.4			426.07
			458.81	461.5			426.07
			458.82	461.5			453.78
			458.83	461.5			453.78
$3\nu_s$	553.77		519.22		538.53		508.20
			519.22				508.20
			519.23				526.26
			519.23				526.26
$2\nu_b$		544.60	533.01	528.7		437.19	431.62
		544.61	533.02	528.9		437.19	431.62
		544.65	533.05	528.9		468.37	460.93
		544.67	533.09	529.1		468.38	460.94
$2\nu_b$		567.31	555.26	545.7		482.53	473.08
		567.31	555.26	545.8		482.58	473.11
		567.32	555.27	545.8		482.66	473.51
		567.32	555.27	545.8		482.67	473.52
		567.33	555.27	547.7		516.72	507.93
		567.33	555.29	547.8		516.74	507.94
		567.36	555.31	547.8		535.97	528.55
		567.38	555.34	547.8		535.98	528.55

^aAll results correspond to the CBB PES of ref 10. 30, (250, 250), and (25, 150, 150) grid points were employed for the 1D(R_{CF}), 2D(θ, φ), and 3D($R_{\text{CF}}, \theta, \varphi$) computations, respectively. ^bFull-dimensional MCTDH results, taken from ref 22.

energies differ by only 1.4 cm^{-1} , indicating that the basis set effects are more significant for this large-amplitude mode. The results of this study show that a rigid monomer intermolecular model using curvilinear internal coordinates can provide good estimates for these large-amplitude low-frequency modes, well separated from the other modes of the system.

In a four-well computation the ground vibrational state of $\text{F}^- - \text{CH}_4$ is split into a global ground state of A_1 symmetry and a triply degenerate F_2 state, where we employ the irreducible representations of the $T_d(M)$ molecular symmetry group to characterize the delocalized vibrational states. The 12D MCTDH study reported that the ground-state tunneling

splitting between the A_1 and F_2 states does not significantly exceed 1 cm^{-1} .²² Our 2D(θ, φ) and 3D($R_{\text{CF}}, \theta, \varphi$) computations show that the ground-state splitting is less than 0.01 cm^{-1} and even for the overtones, e.g., $2\nu_b$, the splittings are not larger than 0.1 cm^{-1} . Thus, the present reduced-dimensional computations predict tunneling splittings orders of magnitude smaller than reported in the 12D MCTDH study. The 3D($R_{\text{CF}}, \theta, \varphi$) splittings are fully converged, but obtained from a rigid monomer model, whereas the MCTDH computations are full-dimensional, but not fully converged. The 3D($R_{\text{CF}}, \theta, \varphi$) study provides energies (in cm^{-1} and setting the zero-point level to 0) for the split ground state as (0.00, 0.00, 0.00, 0.00),

whereas the B1, B2, B3, and B4 basis sets of ref 22 give (0.0, 3.2, 3.2, 3.4), (0.0, 0.8, 1.0, 1.2), (0.0, 0.4, 0.5, 0.5), and (0.0, 0.6, 0.8, 0.9), respectively. The $3D(R_{CF}, \theta, \varphi)$ results reproduce the correct degeneracy of the F_2 state, whereas the MCTDH energies are split even for the F_2 state. The bases from B1 to B3 correspond to increasing size, and as seen above, the splittings tend to vanish as the basis size is increased, although we cannot be confident about the rate of the convergence. It is most likely that the present minuscule splittings would be obtained from a converged full-dimensional study.

For the $F^-CH_2D_2$ complex the $1D(R_{CF})$ model provides a ν_s value of 187.9 cm^{-1} , below the ν_s frequency of F^-CH_4 by only 5.7 cm^{-1} . The two $1D(R_{CF})$ models, in which either the H or D atom connects to F^- , give exactly the same vibrational energy levels. This is the expected behavior because in the $1D(R_{CF})$ model the vibrational Hamiltonian depends only on the total mass of the methane unit; thus, methane can be viewed as a dummy atom with an effective mass of CH_4 or CH_2D_2 . It is important to note that for $J > 0$ calculations this dummy-atom picture does not hold and the rotational levels do depend on the structure and connectivity of the methane unit. The $2D(\theta, \varphi)$ and $3D(R_{CF}, \theta, \varphi)$ models provide vibrational states that can be assigned to either the F^-HCHD_2 or the F^-DCDH_2 minima. Thus, the ground vibrational state is split by 19.1 cm^{-1} and the ν_s and $2\nu_s$ states are split by 18.9 and 18.6 cm^{-1} , respectively. The lower energies correspond to states localized around one of the two F^-DCDH_2 minima. For example, the $1D(R_{CF})$ ν_s fundamental of 187.9 cm^{-1} is split into two 2-fold quasi-degenerate states with energies of 177.9 and 196.8 cm^{-1} corresponding to F^-DCDH_2 and F^-HCHD_2 , respectively. Note that the computation of the rovibrational levels makes the assignment of a vibrational state to one of the minima straightforward, as we will discuss later. For the ν_b fundamental of $F^-CH_2D_2$, the $2D(\theta, \varphi)$ and $3D(R_{CF}, \theta, \varphi)$ results are close to each other, the latter model gives energies lower by about $3\text{--}5\text{ cm}^{-1}$ (6 cm^{-1} for F^-CH_4). For F^-CH_4 the eight ν_b fundamentals are quasi-degenerate around 284.5 cm^{-1} , whereas in the case of $F^-CH_2D_2$ the ν_b energies span a range from 223.7 to 283.8 cm^{-1} in the $3D(R_{CF}, \theta, \varphi)$ model (Table 1).

Hydrogen-Bonded CH and CD Stretching Fundamentals. The spectroscopy of the F^-CH_4 complex was investigated experimentally in the CH stretching region.^{11–13} The most intensive peak in the spectrum corresponds to the hydrogen-bonded CH fundamental (ν_{hb}). The measured ν_{hb} value of 2535 cm^{-1} is significantly red-shifted relative to the ν_1 fundamental of CH_4 (2917 cm^{-1}).¹¹ The ω_{hb} and ω_1 harmonic wavenumbers corresponding to the CBB PES are 2782 and 3018 cm^{-1} , respectively; thus, the harmonic approximation seriously overestimates the ν_{hb} frequency of the complex and underestimates the red shift. The present reduced-dimensional variational results are given in Table 2. The $1D(R_{CH})$ model gives a ν_{hb} value of 2523 cm^{-1} , in excellent agreement with experiment (2535 cm^{-1})¹¹ and the full-dimensional Multimode result (2519 cm^{-1}).¹⁰ Thus, as expected and found previously by Loh et al.,¹² this “local-mode” approximation works very well for the H-bonded CH stretching mode. The coupling between the CH and CF stretching modes is small, because the $2D(R_{CH}, R_{CF})$ model gives a wavenumber of 2527 cm^{-1} . Note that ν_{hb} is above the dissociation energy ($D_0 = 2280\text{ cm}^{-1}$) of F^-CH_4 ; thus, strictly speaking, the CH stretching is a Feshbach resonance. In the $2D(R_{CH}, R_{CF})$ model, we could straightforwardly identify the converged energy level corre-

Table 2. Hydrogen-Bonded CH and CD Stretching Fundamentals (cm^{-1}) of F^-CH_4 and $F^-CH_2D_2$ ^a

	F^-CH_4	F^-HCHD_2	F^-DCDH_2
harmonic	2782	2807	2044
$1D(R_{CH/CD})$	2523	2521	1855
$2D(R_{CH/CD}, R_{CF})$	2527	2517	1905
$12D(\text{Multimode})^b$	2519		
experiment ^c	2535		

^aAll the computed results correspond to the CBB PES of ref 10. ^bFull-dimensional Multimode result taken from ref 10. ^cMeasured value taken from ref 11.

sponding to the ν_{hb} mode and the ν_{hb} wavenumber could be converged with a precision better than 0.01 cm^{-1} applying the code developed for bound-state computations. For the $F^-CH_2D_2$ complex the $1D(R_{CH})$ model gives a CH stretching of 2521 cm^{-1} , whereas the $1D(R_{CD})$ model gives a CD stretching of 1855 cm^{-1} . The corresponding $2D(R_{CH}, R_{CF})$ and $2D(R_{CD}, R_{CF})$ wavenumbers are 2517 and 1905 cm^{-1} , respectively, where the former is again a resonance state, whereas the latter is a bound state. The harmonic analysis performs very poorly for the $F^-CH_2D_2$ complex as well, because the ω_{hb} CH and CD fundamentals are 2807 and 2044 cm^{-1} (on the CBB PES), respectively; i.e., ω_{hb} overestimates the corresponding local-mode energies by $286(\text{CH})$ and $189(\text{CD})\text{ cm}^{-1}$.

Rovibrational Energy Levels. The $J = 1$ and 2 rotational energy levels in the ground and intermolecular fundamental vibrational states of the F^-CH_4 and $F^-CH_2D_2$ complexes are given in Table 3.

The $1D(R_{CF})$ model gives $J = 1$ rotational levels of $0.42(1)$ and $5.50(2)\text{ cm}^{-1}$ for the ground vibrational state of F^-CH_4 , where in parentheses the degeneracies are indicated. Because the $1D(R_{CF})$ model maintains the prescribed C_{3v} point-group symmetry, these rotational levels are in nearly perfect agreement with the energies of a prolate symmetric-top rigid rotor, whereby $A = 5.29\text{ cm}^{-1}$ and $B = C = 0.21\text{ cm}^{-1}$ corresponding to the equilibrium structure of F^-CH_4 . As seen in Table 3, the $1D(R_{CF})$ $J = 2$ rotational energies are also in excellent agreement with the corresponding rigid rotor levels.

In the $2D(\theta, \varphi)$ and $3D(R_{CF}, \theta, \varphi)$ models F^- moves around the CH_4 fragment exploring the T_d -symmetric four-well PES; thus, the C_{3v} symmetry is not maintained anymore. The present calculations show that F^-CH_4 still behaves as a regular symmetric top if the ground or stretching vibrational states are considered. This finding can be explained by the fact that the global wave functions are localized in the vicinity of the minima. However, in the case of the intermolecular bending mode the variational rovibrational computations show substantial splittings of the rigid rotor energy levels. The ($J = 1, K = 0$) and ($J = 2, K = 0$) levels appear, as expected, at $0.43/0.41$ and $1.28/1.24\text{ cm}^{-1}$, respectively, using the $2D(\theta, \varphi)/3D(R_{CF}, \theta, \varphi)$ models; i.e., these levels correspond to slightly perturbed prolate symmetric top energies of $2B$ and $6B$. However, the $K \neq 0$ rotational levels for the degenerate bending mode are substantially split and the splittings are proportional to K . For example, the ($J = 1, K = \pm 1$) level of about 5.4 cm^{-1} is split to 0.00 and 10.92 cm^{-1} , the ($J = 2, K = \pm 1$) level of about 6.2 cm^{-1} is split to 0.83 and 11.75 cm^{-1} , and the ($J = 2, K = \pm 2$) level of about 21.2 cm^{-1} is split to 10.51 and 32.36 cm^{-1} ; thus, the splittings are always $10.92K\text{ cm}^{-1}$. These splittings are due to terms linear in \hat{J} of the rovibrational Hamiltonian. Considerations based on first-order perturbation theory show

Table 3. Rotational Energy Levels (cm^{-1}) Relative to the Corresponding Ground and Fundamental Intermolecular Vibrational States of $\text{F}^- - \text{CH}_4$ and $\text{F}^- - \text{CH}_2\text{D}_2$ Indicating the Degeneracies or Quasi-Degeneracies in Parentheses and the Split Rotational Levels in Bold^a

	$\text{F}^- - \text{CH}_2\text{D}_2$								
	$\text{F}^- - \text{CH}_4$			$\text{F}^- - \text{HCHD}_2$			$\text{F}^- - \text{DCDH}_2$		
	$J = 0$	$J = 1$	$J = 2$	$J = 0$	$J = 1$	$J = 2$	$J = 0$	$J = 1$	$J = 2$
	1D(R_{CF})								
ν_0	0.00(1)	0.42(1)	1.26(1)	0.00(1)	0.38(1)	1.14(1)	0.00(1)	0.40(1)	1.19(1)
		5.50(2)	6.34(2)		3.41(2)	4.17(2)		4.24(2)	5.04(2)
			21.59(2)			13.27(2)			16.58(2)
ν_s	193.55(1)	0.41(1)	1.23(1)	187.90(1)	0.37(1)	1.11(1)	187.90(1)	0.39(1)	1.16(1)
		5.50(2)	6.32(2)		3.41(2)	4.15(2)		4.24(2)	5.02(2)
			21.58(2)			13.26(2)			16.57(2)
	2D(θ, φ)								
ν_0	0.00(4)	0.43(4)	1.28(4)	19.12(2)	0.38(2)	1.15(2)	0.00(2)	0.40(2)	1.21(2)
		5.41(8)	6.26(8)		3.35(4)	4.12(4)		4.16(4)	4.96(4)
			21.21(8)			13.04(4)			16.24(4)
ν_b	290.20(8)	0.00(8)	0.85(8)	259.38(2)	0.38(2)	1.15(2)	226.30(2)	0.40(2)	1.21(2)
		0.43(8)	1.28(8)		3.11(4)	3.88(4)		3.23(4)	4.03(4)
		10.93(8)	10.51(8)			12.10(4)			12.89(4)
			11.78(8)	287.22(2)	0.38(2)	1.15(2)	248.92(2)	0.40(2)	1.21(2)
			32.37(8)		3.66(4)	4.43(4)		5.15(4)	5.96(4)
						14.23(4)			19.83(4)
	3D($R_{\text{CF}}, \theta, \varphi$)								
ν_0	0.00(4)	0.42(4)	1.25(4)	19.11(2)	0.38(2)	1.13(2)	0.00(2)	0.39(2)	1.18(2)
		5.40(8)	6.24(8)		3.35(4)	4.10(4)		4.16(4)	4.94(4)
			21.20(8)			13.03(4)			16.23(4)
ν_s	182.46(4)	0.41(4)	1.22(4)	196.75(2)	0.37(2)	1.10(2)	177.87(2)	0.38(2)	1.15(2)
		5.40(8)	6.21(8)		3.35(4)	4.08(4)		4.15(4)	4.92(4)
			21.20(8)			13.02(4)			16.22(4)
ν_b	284.55(8)	0.00(8)	0.83(8)	254.82(2)	0.38(2)	1.13(2)	223.70(2)	0.39(2)	1.18(2)
		0.41(8)	1.24(8)		3.12(4)	3.87(4)		3.15(4)	3.94(4)
		10.92(8)	10.51(8)			12.14(4)			12.67(4)
			11.75(8)	283.76(2)	0.37(2)	1.12(2)	244.49(2)	0.39(2)	1.18(2)
			32.36(8)		3.65(4)	4.40(4)		5.22(4)	6.00(4)
						14.19(4)			20.04(4)

^aAll the results correspond to the CBB PES of ref 10. 30, (100, 100), and (20, 80, 80) grid points were employed for the 1D(R_{CF}), 2D(θ, φ), and 3D($R_{\text{CF}}, \theta, \varphi$) computations, respectively.

that the terms proportional to \hat{J} have zero contributions for A_1 vibrational states and split the rotational energies by $\varepsilon(\mathbf{v})K$ for E vibrational states, where $\varepsilon(\mathbf{v})$ depends on the vibrational state. The corresponding perturbation theory result for the splitting, $2 \times 2A\zeta K$, where ζ is the Coriolis coupling constant, is well-known for symmetric tops.³⁶ It is thus obvious that these large splittings are caused by neither the interaction between the four minima nor the reduced-dimensions of our models. To further support this statement, we executed 3D($R_{\text{CF}}, \theta, \varphi$) GENIUSH computations restricting the angular DVR grid points into the vicinity of one of the minima and performed 4D and 6D four-well rovibrational computations augmenting the 3D($R_{\text{CF}}, \theta, \varphi$) model by a symmetric CH stretching mode and by the triply degenerate asymmetric stretching mode, respectively. These test computations provided qualitatively the same results as the 3D($R_{\text{CF}}, \theta, \varphi$) four-well computations did, except that the single-well description reduced the quasi-degeneracies by a factor of 4.

We also performed some test rovibrational computations for $\text{F}^- - \text{CH}_4$ in which the rotational–vibrational coupling terms in the \mathbf{G} matrix were neglected (Figure 4). The 1D(R_{CF}) model gave exactly the same energies with and without the rotational–vibrational coupling terms in the Hamiltonian. This can be

readily understood by examining the \mathbf{g} and \mathbf{G} matrices shown in Figure 4. In the 1D(R_{CF}) model both matrices are diagonal; i.e., the rotational–vibrational coupling terms are zero. The rotational block of the \mathbf{G} matrix shows the inverse of the moment of inertia of a symmetric top ($\text{F}^- - \text{CH}_4$). Unlike the 1D(R_{CF}) model, the 2D(θ, φ) and 3D($R_{\text{CF}}, \theta, \varphi$) rovibrational computations provide qualitatively different results with and without rotational–vibrational couplings. When the coupling terms are neglected, all the rotational energies relative to the corresponding vibrational levels become 10.29 and 30.88 cm^{-1} for $J = 1$ and 2, respectively. These values correspond to the rigid rotor energies of the CH_4 unit, whose B value is 5.15 cm^{-1} in the 2D(θ, φ) and 3D($R_{\text{CF}}, \theta, \varphi$) models. Thus, without rotational–vibrational couplings $\text{F}^- - \text{CH}_4$ behaves as a spherical top and the rotational energies are independent of the mass of F^- and distance of F^- from the CH_4 unit. The \mathbf{g} and \mathbf{G} matrices of the 3D($R_{\text{CF}}, \theta, \varphi$) model are also shown in Figure 4. One can observe that the rotational block of the \mathbf{G} matrix corresponds to the inverse of the moment of inertia of the CH_4 unit; i.e., all three diagonal elements are $3/(8m_{\text{H}}r^2)$, where r is the CH distance and m_{H} is the mass of the H atom. In the 2D(θ, φ) and 3D($R_{\text{CF}}, \theta, \varphi$) models the rotational–vibrational couplings have a dramatic effect on the rotational

$$\begin{array}{ccc}
 \mathbf{3D}(R_{CF}, \theta, \varphi) & & \mathbf{1D}(R_{CF}) \\
 \left(\begin{array}{ccccc}
 \frac{m_F M}{m_F + M} & 0 & 0 & 0 & 0 \\
 0 & \frac{m_F M R^2}{m_F + M} & 0 & 0 & 0 \\
 0 & 0 & \frac{m_F M R^2 \sin^2 \theta}{m_F + M} & 0 & 0 \\
 0 & \frac{m_F M R^2 \sin \theta}{m_F + M} & \frac{m_F M R^2 \cos \theta \sin \theta}{m_F + M} & \frac{m_F M R^2 \cos^2 \theta}{m_F + M} & 0 \\
 0 & \frac{m_F M R^2 \sin \theta}{m_F + M} & \frac{m_F M R^2 \cos \theta \sin \theta}{m_F + M} & \frac{m_F M R^2 \cos^2 \theta}{m_F + M} & 0 \\
 0 & 0 & 0 & 0 & \frac{m_F M R^2 \sin^2 \theta}{m_F + M}
 \end{array} \right) & \xrightarrow{\substack{\text{deleting 2nd and 3rd rows and columns} \\ \text{fixing } \theta \text{ and } \varphi \text{ at 0}}} & \left(\begin{array}{cccc}
 \frac{m_F M}{m_F + M} & 0 & 0 & 0 \\
 0 & \frac{8m_H r^2}{3} + \frac{m_F M R^2}{m_F + M} & 0 & 0 \\
 0 & 0 & \frac{8m_H r^2}{3} + \frac{m_F M R^2}{m_F + M} & 0 \\
 0 & 0 & 0 & \frac{8m_H r^2}{3}
 \end{array} \right) \\
 \downarrow \text{inversion } \mathbf{g} & & \downarrow \text{inversion } \mathbf{g} \\
 \left(\begin{array}{ccccc}
 \frac{1}{m_F} + \frac{1}{M} & 0 & 0 & 0 & 0 \\
 0 & \frac{m_F + M}{m_F M R^2} + \frac{3}{8m_H r^2} & 0 & \frac{3 \sin \theta}{8m_H r^2} & -\frac{3 \cos \theta}{8m_H r^2} \\
 0 & 0 & \frac{3m_F M R^2 + 8m_H (m_F + M)r^2}{8m_F m_H M R^2 R^2 \sin^2 \theta} & \frac{3 \cot \theta \cos \theta}{8m_H r^2} & \frac{3 \cot \theta \sin \theta}{8m_H r^2} \\
 0 & \frac{3 \sin \theta}{8m_H r^2} & \frac{3 \cot \theta \cos \theta}{8m_H r^2} & \frac{3}{8m_H r^2} & 0 \\
 0 & -\frac{3 \cos \theta}{8m_H r^2} & \frac{3 \cot \theta \sin \theta}{8m_H r^2} & 0 & \frac{3}{8m_H r^2} \\
 0 & 0 & -\frac{3}{8m_H r^2} & 0 & \frac{3}{8m_H r^2}
 \end{array} \right) & & \left(\begin{array}{cccc}
 \frac{1}{m_F} + \frac{1}{M} & 0 & 0 & 0 \\
 0 & \frac{3(m_F + M)}{3m_F M R^2 + 8m_H (m_F + M)r^2} & 0 & 0 \\
 0 & 0 & \frac{3(m_F + M)}{3m_F M R^2 + 8m_H (m_F + M)r^2} & 0 \\
 0 & 0 & 0 & \frac{3}{8m_H r^2}
 \end{array} \right)
 \end{array}$$

Figure 4. \mathbf{G} and \mathbf{g} matrices for the rovibrational models of F^- – CH_4 with one (R_{CF}) and three (R_{CF}, θ, φ) active vibrational coordinates. The vibrational, rotational, and rotational–vibrational blocks are highlighted with colors black, red, and blue, respectively. M is the mass of $\text{CH}_4(T_d)$; r and R denote the CH and CF distances, respectively; and θ and φ are the polar angles of F^- . For the sake of simplicity the matrices correspond to the body-fixed frame in which one of the H atoms is in the z axis and another H atom is in the xz plane and then the system is moved into the center of mass frame. The actual $3\text{D}(R_{CF}, \theta, \varphi)$ computations are performed in the frame shown in Figure 2.

energies and change qualitatively the rotational spectrum from that of a spherical top to that of a symmetric top molecule.

As to the F^- – CH_2D_2 complex, we can define two different asymmetric rotors (C_2 point-group symmetry) having either a F^- – HCHD_2 or a F^- – DCDH_2 connectivity. Both of them are very close to the symmetric top limit, because the equilibrium rotational constants (A , B , C), in cm^{-1} , are (3.223, 0.193, 0.190) and (4.046, 0.202, 0.199), respectively. Unlike the vibrational energy levels, the rotational levels do depend on the connectivity used in the $1\text{D}(R_{CF})$ model. For the ground vibrational state of F^- – HCHD_2 , the $1\text{D}(R_{CF})$ model gives $J = 1$ rotational energies of 0.38(1) and 3.41(2) cm^{-1} , whereas the corresponding values are 0.40(1) and 4.24(2) cm^{-1} for F^- – DCDH_2 , where the quasi-degeneracies are indicated in parentheses. As mentioned earlier, in the $2\text{D}(\theta, \varphi)$ and $3\text{D}(R_{CF}, \theta, \varphi)$ models the vibrational ground state is split by 19.1 cm^{-1} . Because the rotational levels for the vibrational state at 19.1 cm^{-1} are 0.38 and 3.35 cm^{-1} , we can assign the vibrational level of 19.1 cm^{-1} to the F^- – HCHD_2 minimum on the basis of the $1\text{D}(R_{CF})$ rotational energies, where the connectivity in the model is well-defined. On the basis of similar considerations we can assign each rovibrational level of F^- – CH_2D_2 to either F^- – HCHD_2 or F^- – DCDH_2 structures, as seen in Table 3. Similar to F^- – CH_4 , the rotational levels in the ground and stretching excited states can be well characterized by rigid rotor levels, whereas substantial splittings of the rigid rotor energies are found for some of the rotational levels in the intermolecular bending vibrational states.

SUMMARY AND CONCLUSIONS

Following the full-dimensional vibration-only computations carried out by the Eckart–Watson–operator-based Multimode approach in 2008¹⁰ and the MCTDH approach in 2012,²² we

performed reduced-dimensional rovibrational computations for F^- – CH_4 and F^- – CH_2D_2 using the ab initio CBB PES.¹⁰ The CBB PES is invariant under permutation of identical atoms; thus, the PES describes all four equivalent minima of the complex. Several reduced-dimensional models were implemented into the general rovibrational code GENIUSH,^{24,25} which computes the complicated form of the kinetic energy operator numerically. Because we used curvilinear polyspherical coordinates, our $2\text{D}(\theta, \varphi)$ and $3\text{D}(R_{CF}, \theta, \varphi)$ models could describe the four-well rovibrational dynamics of the complexes and the low-frequency intermolecular modes could be fully converged. The present results highlight the painfully slow convergence of the rectilinear–normal–coordinates-based approaches for the large amplitude intermolecular modes. The $3\text{D}(R_{CF}, \theta, \varphi)$ intermolecular rigid monomer model provides vibrational energies for F^- – CH_4 in good agreement (less than 15 cm^{-1} differences) with the full-dimensional MCTDH results. We expect similar accuracy for the F^- – CH_2D_2 complex, which has not been studied thus far. The present four-well calculations predict negligible tunneling splittings, less than 0.01 cm^{-1} , for the low-lying intermolecular vibrational states of F^- – CH_4 ; thereby setting a significantly lower upper limit of the splittings than the MCTDH upper boundary of about 1 cm^{-1} . The present results are converged but of reduced dimensionality, whereas the MCTDH study is full-dimensional, but not fully converged. Further studies, both experimental and theoretical, would be required to confirm the splitting values computed in this study.

Multimode calculations performed by one of us provided full-dimensional benchmark results corresponding to the CBB PES for the intramolecular vibrations of the CH_4 fragment of the F^- – CH_4 complex.¹⁰ The computed Multimode frequencies were in excellent agreement with the available experimental

data in the CH stretching region.^{10–13} The present 1D(R_{CH}) calculations show that a simple local-mode model provides a hydrogen-bonded CH stretching fundamental of 2523 cm^{-1} , in excellent agreement with the full-dimensional Multimode result of 2519 cm^{-1} .¹⁰ Therefore, our predictions of 2521 and 1855 cm^{-1} for the CH and CD stretching fundamentals, respectively, of the F^- - CH_2D_2 complex are expected to be accurate as well.

GENIUSH allows adding the rotational motion to reduced-dimensional models;²⁵ thus, we have performed computations for the $J = 1$ and 2 rovibrational states. For the ground and stretching vibrational states having A_1 symmetry within a local single-well model, the rotational levels of F^- - CH_4 are very similar to the corresponding prolate symmetric-top rigid-rotor energies. For the intermolecular bending mode, which has E symmetry in a single-well description, we found exceedingly large splittings of the $K \neq 0$ rigid rotor energies. In the 2D(θ, φ) and 3D($R_{\text{CF}}, \theta, \varphi$) models of F^- - CH_2D_2 the vibrational levels are split into states which can be assigned to either F^- -H or F^- -D connectivity. The computed rovibrational energies and the differences in the rotational constants of the F^- -HCHD₂ and F^- -DCDH₂ complexes provide a straightforward guidance to assign the vibrational states to either minimum.

AUTHOR INFORMATION

Corresponding Author

*E-mail: czako@chem.elte.hu.

Notes

The authors declare no competing financial interest.

ACKNOWLEDGMENTS

This work was supported by the Scientific Research Fund of Hungary (OTKA) through Grant No. NK83583 and an ERA-Chemistry grant (NN 81072). G.C. also thanks the Magyar Fellowship of the European Union and Hungary (TÁMOP 4.2.4.A/1-11-1-2012-0001) for financial support.

REFERENCES

- (1) Czakó, G.; Bowman, J. M. CH Stretching Excitation Steers the F Atom to the CD Bond in the $\text{F} + \text{CHD}_3$ Reaction. *J. Am. Chem. Soc.* **2009**, *131*, 17534–17535.
- (2) Czakó, G.; Bowman, J. M. Dynamics of the Reaction of Methane with Chlorine Atom on an Accurate Potential Energy Surface. *Science* **2011**, *334*, 343–346.
- (3) Czakó, G.; Bowman, J. M. Accurate ab Initio Potential Energy Surface, Thermochemistry, and Dynamics of the $\text{Cl}(^2\text{P}, ^2\text{P}_{3/2}) + \text{CH}_4 \rightarrow \text{HCl} + \text{CH}_3$ and $\text{H} + \text{CH}_3\text{Cl}$ Reactions. *J. Chem. Phys.* **2012**, *136*, 044307.
- (4) Zhang, W.; Kawamata, H.; Liu, K. CH Stretching Excitation in the Early Barrier $\text{F} + \text{CHD}_3$ Reaction Inhibits CH Bond Cleavage. *Science* **2009**, *325*, 303–306.
- (5) Kawamata, H.; Zhang, W.; Liu, K. Imaging the Effects of the Antisymmetric Stretch Excitation of CH_4 in the Reaction with F Atom. *Faraday Discuss.* **2012**, *157*, 89–100.
- (6) Troya, D. Ab initio and Direct Quasiclassical-Trajectory Study of the $\text{F} + \text{CH}_4 \rightarrow \text{HF} + \text{CH}_3$ Reaction. *J. Chem. Phys.* **2005**, *123*, 214305.
- (7) von Horsten, H. F.; Clary, D. C. Reactive Resonances in the $\text{F} + \text{CHD}_3$ Reaction—A Quantum Dynamics Study. *Phys. Chem. Chem. Phys.* **2011**, *13*, 4340–4356.
- (8) Espinosa-García, J.; Bravo, J. L.; Rangel, C. New Analytical Potential Energy Surface for the $\text{F}(^2\text{P}) + \text{CH}_4$ Hydrogen Abstraction Reaction: Kinetics and Dynamics. *J. Phys. Chem. A* **2007**, *111*, 2761–2771.
- (9) Czakó, G.; Shepler, B. C.; Braams, B. J.; Bowman, J. M. Accurate ab Initio Potential Energy Surface, Dynamics, and Thermochemistry of the $\text{F} + \text{CH}_4 \rightarrow \text{HF} + \text{CH}_3$ Reaction. *J. Chem. Phys.* **2009**, *130*, 084301.

(10) Czakó, G.; Braams, B. J.; Bowman, J. M. Accurate ab Initio Structure, Dissociation Energy, and Vibrational Spectroscopy of the F^- - CH_4 Anion Complex. *J. Phys. Chem. A* **2008**, *112*, 7466–7472.

(11) Wild, D. A.; Loh, Z. M.; Bieske, E. J. Infrared Spectra of the F^- - CH_4 and Br^- - CH_4 Anion Complexes. *Int. J. Mass. Spectrom.* **2002**, *220*, 273–280.

(12) Loh, Z. M.; Wilson, R. L.; Wild, D. A.; Bieske, E. J.; Gordon, M. S. Structures of F^- - $(\text{CH}_4)_n$ and Cl^- - $(\text{CH}_4)_n$ ($n = 1, 2$) Anion Clusters Elucidated through Ab Initio Calculations and Infrared Spectra. *Aust. J. Chem.* **2004**, *57*, 1157–1160.

(13) Loh, Z. M.; Wilson, R. L.; Wild, D. A.; Bieske, E. J.; Lisy, J. M.; Njagic, B.; Gordon, M. S. Infrared Spectra and Ab Initio Calculations for the F^- - $(\text{CH}_4)_n$ ($n = 1-8$) Anion Clusters. *J. Phys. Chem. A* **2006**, *110*, 13736–13743.

(14) Neumark, D. M. Slow Electron Velocity-Map Imaging of Negative Ions: Applications to Spectroscopy and Dynamics. *J. Phys. Chem. A* **2008**, *112*, 13287–13301.

(15) Cheng, M.; Feng, Y.; Du, Y.; Zhu, Q.; Zheng, W.; Czakó, G.; Bowman, J. M. Communication: Probing the Entrance Channels of the $\text{X} + \text{CH}_4 \rightarrow \text{HX} + \text{CH}_3$ ($\text{X} = \text{F}, \text{Cl}, \text{Br}, \text{I}$) Reactions Via Photodetachment of X^- - CH_4 . *J. Chem. Phys.* **2011**, *134*, 191102.

(16) Yacovitch, T. I.; Garand, E.; Kim, J. B.; Hock, C.; Theis, T.; Neumark, D. M. Vibrationally Resolved Transition State Spectroscopy of the $\text{F} + \text{H}_2$ and $\text{F} + \text{CH}_4$ Reactions. *Faraday Discuss.* **2012**, *157*, 399–414.

(17) Carter, S.; Bowman, J. M.; Handy, N. C. Extensions and Tests of "Multimode": A Code To Obtain Accurate Vibration/Rotation Energies of Many-Mode Molecules. *Theor. Chem. Acc.* **1998**, *100*, 191–198.

(18) Eckart, C. Some Studies Concerning Rotating Axes and Polyatomic Molecules. *Phys. Rev.* **1935**, *47*, 552–558.

(19) Watson, J. K. G. Simplification of the Molecular Vibration–Rotation Hamiltonian. *Mol. Phys.* **1968**, *15*, 479–490.

(20) Meyer, H.-D.; Manthe, U.; Cederbaum, L. S. The Multi-Configurational Time-Dependent Hartree Approach. *Chem. Phys. Lett.* **1990**, *165*, 73–78.

(21) Beck, M. H.; Jäckle, A.; Worth, G. A.; Meyer, H.-D. The Multiconfiguration Time-Dependent Hartree (MCTDH) Method: A Highly Efficient Algorithm for Propagating Wavepackets. *Phys. Rep.* **2000**, *324*, 1–105.

(22) Wodraszka, R.; Palma, J.; Manthe, U. Vibrational Dynamics of the CH_4F^- Complex. *J. Phys. Chem. A* **2012**, *116*, 11249–11259.

(23) Császár, A. G.; Fábri, C.; Szidarovszky, T.; Mátyus, E.; Furtenbacher, T.; Czakó, G. The Fourth Age of Quantum Chemistry: Molecules in Motion. *Phys. Chem. Chem. Phys.* **2012**, *14*, 1085–1106.

(24) Mátyus, E.; Czakó, G.; Császár, A. G. Toward Black-Box-Type Full- and Reduced-Dimensional Variational (Ro)vibrational Computations. *J. Chem. Phys.* **2009**, *130*, 134112.

(25) Fábri, C.; Mátyus, E.; Császár, A. G. Rotating Full- and Reduced-Dimensional Quantum Chemical Models of Molecules. *J. Chem. Phys.* **2011**, *134*, 074105.

(26) Carrington, T., Jr.; Wang, X. G. Computing Ro-Vibrational Spectra of van der Waals Molecules. *WIREs Comput. Mol. Sci.* **2011**, *1*, 952–963.

(27) Brown, J.; Wang, X. G.; Dawes, R.; Carrington, T., Jr. Computational Study of the Rovibrational Spectrum of $(\text{OCS})_2$. *J. Chem. Phys.* **2012**, *136*, 134306.

(28) Jankowski, P.; McKellar, A. R. W.; Szalewicz, K. Theory Untangles the High-Resolution Infrared Spectrum of the *ortho*- H_2 -CO van der Waals Complex. *Science* **2012**, *336*, 1147–1150.

(29) Podolsky, B. Quantum–Mechanically Correct Form of Hamiltonian Function for Conservative Systems. *Phys. Rev.* **1928**, *32*, 812–816.

(30) Watson, J. K. G. The Molecular Vibration–Rotation Kinetic-Energy Operator for General Internal Coordinates. *J. Mol. Spectrosc.* **2004**, *228*, 645–658.

(31) Harris, D. O.; Engerholm, G. G.; Gwinn, W. D. Calculation of Matrix Elements for One–Dimensional Quantum–Mechanical

Problems and the Application to Anharmonic Oscillators. *J. Chem. Phys.* **1965**, *43*, 1515–1517.

(32) Lanczos, C. An Iteration Method for the Solution of the Eigenvalue Problem of Linear Differential and Integral Operators. *J. Res. Natl. Bur. Stand.* **1950**, *45*, 255–282.

(33) Echave, J.; Clary, D. C. Potential Optimized Discrete Variable Representation. *Chem. Phys. Lett.* **1992**, *190*, 225–230.

(34) Wei, H.; Carrington, T., Jr. The Discrete Variable Representation of a Triatomic Hamiltonian in Bond Length–Bond Angle Coordinates. *J. Chem. Phys.* **1992**, *97*, 3029–3037.

(35) Szalay, V.; Czako, G.; Nagy, A.; Furtenbacher, T.; Császár, A. G. On One-Dimensional Discrete Variable Representations with General Basis Functions. *J. Chem. Phys.* **2003**, *119*, 10512–10518.

(36) Papousek, D.; Aliev, M. R. *Molecular Vibrational-Rotational Spectra*; Elsevier; Amsterdam, 1982.